Nanoscale

Accepted Manuscript

This article can be cited before page numbers have been issued, to do this please use: J. Méndez-Ramos, A. Menendez Velazquez, F. J. del Castillo Vargas, M. Medina-Alayón, A. B. García-Delgado, S. Torres-García, P. Acosta-Mora, C. Mullins, E. Borges and P. Esparza, *Nanoscale*, 2025, DOI: 10.1039/D5NR03289J.

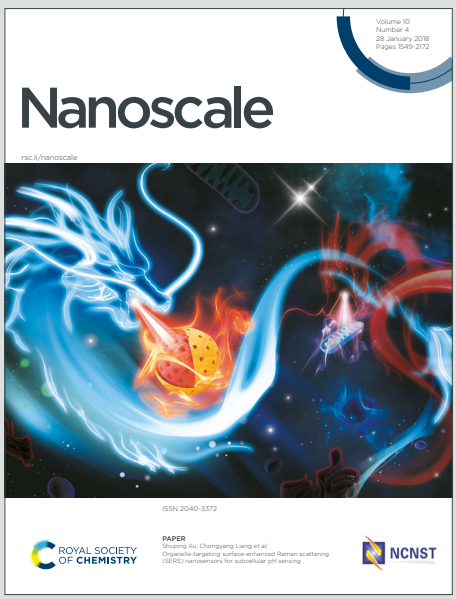

ROYAL SOCIETY OF CHEMISTRY

rsc.li/nanoscale

View Article Online
DOI: 10.1039/D5NR03289J

ARTICLE

"In Rust we Shine": an all-in-one photo-electrocatalytic device for low-cost infrared-induced hematite's water-splitting with polymeric EVA film containing rare-earth up-conversion particles

Received 00th January 20xx,
Accepted 00th January 20xx

DOI: 10.1039/x0xx00000x

J.Méndez-Ramos[a,b*], A.Menéndez-Velázquez[c*], J.del-Castillo[b], M.Medina-Alayón[a,b], A.B. García-Delgado[c], S.Torres-García[a,b], P.Acosta-Mora[a,b] M.E. Borges[d] , C.B. Mullins[e] and P. Esparza[f]*

Handling and transforming solar radiation with spectral conversion luminescent materials constitutes a frontier approach in photonic research for advancing environmental catalysis and sustainable hydrogen production via photocatalytic water-splitting. In this study, a photon-assisted approach is used to enhance the photocatalytic activity of hematite (α-Fe_2O_3) photoelectrodes using Yb^{3+} and Er^{3+} co-doped $NaYF_4$ particles. These particles emit intense green light through near infrared-to-visible up-conversion, with emission wavelengths well aligned with the bandgap of hematite, thereby optimizing photo-electrochemical water-splitting. Moreover, luminescent ethylene-vinyl acetate (EVA) films embedded with up-conversion particles were fabricated and utilized to manufacture laminated glass structures, with hematite coated on the opposite side. This all-in-one photonic device serves as a proof of concept for an industrially relevant platform enabling low-cost infrared-driven water-splitting. Photocurrent generation in this system is driven exclusively by mainly green upconverted photons under excitation from the 980-nm diode laser, which are absorbed by the hematite layer. The resulting up-converted green light coming out from the EVA film triggers surface oxidation on the hematite photocatalyst, demonstrating that water-spitting can be achieved through the up-conversion luminescence alone. Thus, we are proving that even with low energy green and red upconversion emission, it is possible to enable up-conversion driven water-splitting reactions.

Introduction

Bio-inspiration of photosynthesis leads the way for solar-driven-hydrogen energy renewable source: sunlight can be used to rearrange the low energy bonds of water into high energy bonds of hydrogen and oxygen to store energy, like the chloroplasts of plants do [1,2]. The use of the long infrared tail of the incident solar radiation has untapped and crucial applications in photocatalysis and energy harvesting schemes [3]. *"There is plenty of energy at the bottom"*, paraphrasing the revered professor Feynman, paves the way for harvesting the large infrared tail of the incident sun´s irradiation, aimed at photocatalytic applications [4,5]. Handling and transforming incoming sun´s infrared radiation (which accounts for more than 50 % of solar energy) with up-conversion luminescent materials [6] constitute a frontier approach in photonic research used to boost hydrogen production via photocatalytic water-splitting in photo-electrochemical cell (PEC) [7]. Up-conversion luminescence processes act *like a bridge over troubled* gaps [8], in this case, providing extra photons for absorption by catalysts bridging the large bandgap of photocatalytic semiconductors as a not yet fully explored highway.

One of the most useful and interesting photoelectrodes is hematite (α-Fe_2O_3), since it has garnered significant attention due to its abundance, low cost, stability, non-toxic nature and its electronic band gap suitable for efficient absorption of visible light in a photo-electrochemical cell (PEC) [9-10]. Hematite has been identified as one of the most promising photoanode materials [11, 12], since its absorption range lies in the visible region up to around 610 nm [9], which makes it an accurate candidate for solar energy conversion utilized in PEC water-splitting [13, 14]. Thus, to further improve its photocatalytic efficiency, up-conversion processes are the key factor to convert infrared radiation into the hematite absorption wavelength range. Incorporating up-conversion rare-earth doped materials, in particular, high efficient Yb^{3+}-Er^{3+} co-doped $NaYF_4$ particles, will enable the absorption of near-infrared light, which is then re-emitted mainly as green

[a]*Departamento de Física, Universidad de La Laguna, Tenerife, Spain*
[b]*Instituto Universitario de Materiales y Nanotecnología, Universidad de La Laguna, Tenerife, Spain.*
[c]*Unidad de Materiales Fotoactivos, Centro Tecnológico IDONIAL, 33417 Avilés, Asturias, Spain*
[d]*Departamento de Ingeniería Química, Universidad de La Laguna, Tenerife, Spain*
[e]*Department of Chemistry; Texas Materials Institute; McKetta Department of Chemical Engineering, The University of Texas at Austin, Austin, Texas 78712, United States*
[f]*Departamento de Química Inorgánica, Universidad de La Laguna, Tenerife, Spain*
*corresponding authors: jmendezr@ull.edu.es, pesparza@ull.edu.es , amador.menendez@idonial.com
†. Supplementary Information available: See DOI: 10.1039/x0xx00000x

photons [5,15]. These additional photons could be absorbed by hematite, thus improving its efficiency in the water-splitting process. Here we explore this potential way to enhance hematite's performance in solar energy applications, absorbing near-infrared radiation and emitting in the visible range [16], so more photons could be provided for absorption by the hematite photoelectrodes for water-splitting [9,12,17]. Our approach can shine a light on the state of the art of up-conversion sensitized photocatalysis since in the last years, there has been an increasing number of published works, where up-conversion effect is largely assumed, unfortunately misinterpreted in many cases, as pointed out by Prof. Cates and co-workers in [18], rather than proven experimentally [19,20]. In this work, we emphasize the sole role of the photonic up-conversion effect on the infrared-driven boosted photocatalytic reactions, disregarding any possible side effects [5, 8]. A 980 nm laser has been used as the only excitation source for achieving PEC water-splitting. This set-up proves that activation of α-Fe_2O_3 photocatalyst occurs only under NIR irradiation up-converted into suitable green photons. Thus we present the role of a solely up-conversion luminescent effect to split water over a hematite´s photoelectrode: "in rust we shine".

Also in this work, we present a quite significant added value which is related to the integration method of our up-conversion agent, solvothermal $NaYF_4$:Yb^{3+},Er^{3+} micro-sized particles [21], within the PEC setup and the hematite photoelectrode. In detail, an ethylene vinyl acetate (EVA) thermoplastic copolymer film has been doped with up-conversion particles, forming luminescent EVA layers. These layers were then used to manufacture laminated glass, with hematite coated on the opposite side. EVA is widely recognized for its excellent optical and mechanical properties and is commonly used in conventional silicon and thin film photovoltaic solar (PV) cells as a protective polymer layer that shields against environmental degradation, particularly from moisture [22]. At the same time, EVA has high transmittance in the visible / NIR region of the spectrum, ensuring that it does not block sunlight that would otherwise reach the solar cells. These attributes are crucial to the objectives of this study. First, EVA's resistance to moisture enables its application in aquatic or humid environments. Second, its high transmittance in the visible-NIR range minimizes parasitic absorption of both incoming NIR light and up-converted visible emission. In addition, EVA offers excellent chemical and optical compatibility as a host matrix for luminescent species, maintaining—or at least not significantly quenching—their luminescent properties during the transition from solution to solid state [23]. In particular, the EVA polymer demonstrated good compatibility with the luminescent agent investigated in this work. Overall, the use of EVA in this system represents a proof of concept of this all-in-one photonic device for low-cost infrared-induced hydrogen generation via water splitting.

Experimental

Hematite (α-Fe_2O_3)-photoanode preparation

The synthesis procedure consists in growing the well-ordered and oriented iron oxide nanorods layer onto transparent conducting polycrystalline substrate to study its optical and photo-electrochemical properties. The growth of the three-dimensional array of crystalline highly oriented hematite nanorod bundles was conducted according to ref. [24]. The preparation was performed with reagent grade chemicals. An aqueous solution (Milli Q water) of 0.15 M of ferric chloride ($FeCl_3 \cdot 6H_2O$, Scharlau 99%) and 1M of sodium nitrate ($NaNO_3$, Scharlau 99%) containing a polycrystalline FTO substrate (F–SnO_2) (1,1 mm of thickness, 7 Ω/cm^2) was heated in autoclave by hydrothermal synthesis method at a constant temperature of 100 °C for 5h. Subsequently, the thin films formed are thoroughly washed with water to remove any residual salts. A second heat-treatment in air at 500 °C for 2 h is performed to obtain the pure translucent brown thin film thermodynamically stable crystallographic phase of ferric oxide (α-Fe_2O_3). In-depth description of preparation of the photoanode is presented in ESI†.

$$FeCl_3 + H_2O \xrightarrow[100^\circ C]{} \alpha\text{-FeOOH} + \beta\text{-FeOOH} + HCl + H_2O$$

$$\alpha\text{-FeOOH} + \beta\text{-FeOOH} \xrightarrow[500\ ^\circ C, 2\ h]{} \alpha\text{-}Fe_2O_3$$

Synthesis of solvothermal $NaYF_4$:Yb^{3+},Er^{3+} up-conversion micro-sized particles

Micro-sized particles with composition $NaY_{0.93}Yb_{0.05}Er_{0.02}F_4$ were obtained by solvothermal method described as follows [25]. Oleic acid (90%), erbium acetate ($(CH_3COO)_3Er$, 99.9%), yttrium acetate ($(CH_3COO)_3Y$, 99.9%), ytterbium(III) chloride hexahydrate ($YbCl_3 \cdot 6H_2O$, 99.998%), sodium hydroxide (NaOH, 97%), ammonium fluoride (NH_4F, 98%) and ethanol (Anhydrous) were purchased from Sigma Aldrich and used as purchased: Briefly, a transparent homogeneous solution was conducted by vigorous stirring of 2 ml aqueous solution containing 0.3 g NaOH, 10 ml ethanol and 20 ml oleic acid. Next, 2 ml aqueous solution containing 0.485 mmol of $Y(CH_3COO)_3$, 0.025 mmol of $YbCl_3 \cdot 6H_2O$ and 0.01 mmol of $Er(CH_3COO)_3 \cdot H_2O$, were added to the above solution. Finally, 2 ml aqueous solution containing 2 mmol of NH_4F were added, and after stirring for about 30 min, the as-obtained homogeneous colloidal solution was transferred into a 50 ml stainless Teflon-lined autoclave, sealed, and kept at 220 °C for 24 h. The autoclave was naturally cooled down to room temperature. The precipitate deposited at the bottom of Teflon vessel was collected by centrifugation. Then, it was washed twice by re-dispersing in 4 ml cyclohexane, followed by precipitation with 8 ml ethanol. Finally, it was recovered using centrifugation and air-dried at 60 °C for 12 h.

Fabrication of luminescent and non-luminescent EVA films followed by glass lamination

This section outlines the fabrication of luminescent ethylene-vinyl acetate (EVA) films-doped with different $NaYF_4$ up-conversion particles and non-luminescent EVA films, followed by glass lamination.

Initially, EVA pellets were dissolved in toluene under constant stirring at 80 °C until complete dissolution was achieved. $NaYF_4$ up-conversion particle powder was then added to the solution, followed by vigorous mixing to ensure homogeneous dispersion. The resulting mixture contained different amounts rare-earth doped $NaYF_4$ particles: 2.5, 5 and 10 wt%, calculated relative to the EVA content.

Once uniform dispersion was attained, the solvent was evaporated to reach solid EVA films doped with $NaYF_4$ particles. These films were then processed using a hot-plate press, applying controlled pressure and temperature to ensure uniformity and to produce films with varying thicknesses. The optimal configuration consisted of EVA films containing 5 wt% $NaYF_4$ particles with a thickness of 1 mm, as it will be proved in the following section.

In parallel, control (non-luminescent) EVA films were prepared using the same method, serving as reference samples for subsequent optical characterization.

All EVA films were subsequently used in the fabrication of laminated glass structures, with a hematite coating on the opposite side of the glass. Glass substrates were laminated, each incorporating a specific type of luminescent EVA film that covered only a portion of the glass surface. The remaining area was laminated with undoped EVA, serving as a reference for comparative optical characterization, as mentioned. The lamination process was carried out at an optimized temperature of 90 °C and a pressure of approximately 700 mbar, ensuring strong adhesion while preventing thermal degradation of the EVA matrix, the luminescent particles, and the hematite coating.

A 3-D infographic schematic model of our envisaged approach aimed at hematite's water-splitting assisted by up-conversion luminescence, "in rust we shine", is depicted in Fig 1. Moreover, schematic illustrations of the luminescent EVA film preparation process is presented in Fig. 2, along with real photographs of the compact device comprising hematite photoelectrodes laminated with luminescent EVA film, showing intense green up-conversion emission due to rare-earth doped $NaYF_4$ particles under 980 nm laser excitation. It should be noticed that the particles are intrinsically luminescent in their solid (powder) form. When introduced into a liquid medium, the particles do not dissolve but rather form a dispersion. In this dispersed state, they maintain their individual integrity and optical properties, and the photoluminescence is largely preserved due to the absence of strong interparticle interactions or aggregation that could lead to quenching mechanisms. After the film formation via solvent casting, the particles transition back into the solid state while being embedded within the host matrix. In this process, they essentially recover their original solid-state configuration, where they are again spatially isolated as in the initial powder form. Crucially, there is no chemical interaction or significant physical perturbation between the particles and the surrounding matrix material that would alter their emissive properties. The matrix acts as a passive medium and does not introduce pathways for non-radiative decay. To support this assumption we have compared emission properties of the solid microparticles in solution and when embedded in the EVA polymer after the casting process (see Fig S1 presented in ESI†). As it can be clearly seen, the emission profiles are identical, demonstrating that the EVA polymer matrix acts as a passive medium and does not interfere with the intrinsic luminescence of the microparticles.

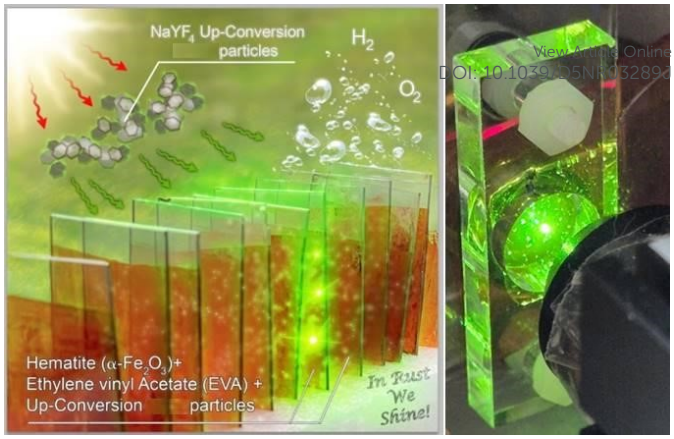

Fig.1 3D infographic model of envisaged approach aimed at hematite's water splitting assisted by up-conversion luminescence, "in rust we shine", along with real photographs of luminescent EVA film laminated over the hematite photoelectrode.

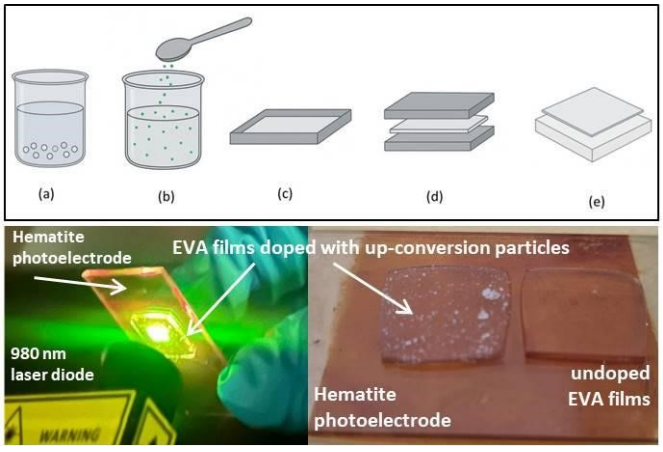

Fig.2 Schematic illustrations of the luminescent EVA film preparation process. Upper images: (a) Dissolution of EVA pellets in toluene; (b) Addition of up-converter particles to the EVA solution and dispersion; (c) Formation of luminescent EVA layers via the solvent casting process; (d) Final luminescent EVA layers obtained through hot-pressing; (e) Glass laminated with the luminescent EVA layer. Bottom images: Real photographs showing intense green up-conversion under NIR 980nm laser diode excitation coming from rare-earth doped $NaYF_4$ particles embedded in EVA films, as all-in-one photonic device.

View Article Online
DOI: 10.1039/D5NR03480J

Up-conversion luminescence characterization

Up-conversion measurements were carried out with a continuous wave infrared collimated laser diode at 980 nm with a power up to 300 mW, and focused over the sample using a 4x micro-objective, with a focal length of 4.51 mm and 0.55 of numerical aperture, which led to a micron-size area for laser spot over the sample and therefore with a very intense power density [4,5]. Detection was carried out with a 0.25 m monochromator equipped with a photomultiplier tube. A 4× microscope objective lens was used for concentrating incident laser radiation onto the samples. All spectra were collected at room temperature and corrected by instrumental response.

Structural characterization

The XRD measurements were carried out with a Philips Panalytical X'Pert Pro diffractometer (with a primary monochromator, a Cu Kα1 radiation source (λ =1.5406 Å) and an X'Celerator detector). XRD patterns were collected with a step of 0.016º in the 2θ angular range (10-80º) during 30 min. LaB_6 was used as internal standard diffraction pattern to calibrate the parameters of the instrumental profile. For $NaYF_4$ particles, TEM images and EDS measurements were obtained by a transmission electron microscope (JEOL-JEM 1400), with a field emission gun, operating at 100 kV and a point-to-point resolution of 0.44 nm.

The analyzed samples were prepared in acetone and finally dropping them onto carbon-coated copper grids. The microstructure of the (α-Fe_2O_3)-photoanode was examined by scanning electron microscopy (SEM) (ZEISS EVO 15) operating at 200 kV. The equipment used an Oxford Link detector to perform energy-dispersive X-ray spectroscopy analysis (EDX) Oxford X-MAX. The corresponding UV–vis spectra were recorded with a UV–vis spectrometer (Varian Cary 3 UV–vis spectrometer) equipped with an integration sphere. The spectra were recorded in diffuse reflectance mode and transformed to Kubelka–Munk units.

Up-conversion powered photo-electrochemical (PEC) cell setup

The experimental setup of the photo-electrochemical (PEC) cell used in this work comprised a quartz-made container with a specific shape holding three electrodes (working electrode, counter electrode, and reference) submerged in an electrolyte [5, 7]. The working electrode (photoanode) consisting of α-Fe_2O_3 on an FTO glass whose exposed surface is 0.38 cm^2. The counter electrode is a platinum spiral thread produces Hydrogen gas (H_2). The third electrode is the reference, made of Silver/Silver Chloride (Ag/AgCl) in a saturated solution of Potassium chloride (KCl). When light strikes the surface of this semiconductor it excites electrons from the valence band to the conduction band, creating electron-hole pairs, and the electrons are transferred to the electrolyte while the holes remain in the photoelectrode. The electrolyte used in this process is typically a solution of potassium hydroxide (in this case a KOH solution 1M), which acts as a conductive medium between the anode and cathode. The KOH alkaline solution also serves as a source of OH^- which is transformed to O_2 in the photoanode, producing the necessary electrons to induce hydrogen generation at the cathode. The counter electrode completes the circuit and allows the flow of electrons, resulting in the generation of an electrical current. A potentiostat (AMEL System 5000) is connected to the PEC cell to measure the obtained photocurrent, which is recorded. Measured potentials versus the reference are referred to the Reversible Hydrogen Electrode (RHE), which is given by:

$$E\ (\text{vs. RHE}) = E(\text{vs. Ag/AgClsat}) + E^{o}\ \text{Ag/AgClsat} + 0{,}0591 \times \text{pH}$$

A constant anodic potential of 0.21V vs. Ag/AgClsat (it means, 1.23V vs. RHE with an alkaline pH of 14, being E^o Ag/AgClsat = 0.197 V) has been applied.

Under standard conditions water can be electrolysed with an electrical potential of 1.23 V vs RHE. The reaction in a PEC cell [7] can be summarized as: $H_2O + h\nu \rightarrow H_2 + ½\ O_2$. The electrochemical decomposition of water can only happens when the potential gap $\Delta E \geq 1.23$ eV, so it will take place only when the energy of the absorbed incident photon on the photoelectrode surface is equal or greater than that potential. In an alkaline solution, the overall water-splitting reaction consists of two half reactions: Oxygen Evolution Reaction (OER) and the Hydrogen evolution reaction (HER):

$$4\ OH^- \rightarrow O_2 + 2H_2O + 4e^-\ (\text{OER});\quad 4H_2O + 4e^- \rightarrow 2H_2 + 4\ OH^-\ (\text{HER})$$

The anodic photocurrent is measured as the result of the OER. The photoelectrolysis has been carried out under a 980 nm laser diode with a power up of 300 mW focused over the sample using a 4x microscope objective lens.

Results and Discussion

Structural characterization

First, we present a detailed structural characterization of the backbone of the photo-electrochemical set-up, that is, the hematite (α-Fe_2O_3) photoanode, presented in ESI†. Figure S2 in Suppl. Info shows scanning electron microscopy (SEM) images of the synthesized (α-Fe_2O_3)-photoanode, showing a homogeneous hematite layer formed by an oriented structure of nanorods of about 50 nm in diameter. Figure S1 also shows the cross-sectional image, indicating the mean thickness of the thin films of about 1.4 μm of thickness. EDX spectra of the synthesized sample show that all samples have composed of Fe, Sn, O and small amount of Si elements. The corresponding inset table in Fig. S2 shows the atomic elemental composition. Accordingly, the sample is formed by hematite (α-Fe_2O_3) on the SnO_2 film surface. The small amount of Si detected

corresponds to SiO_2 glass substrate. Finally, X-ray diffraction (XRD) pattern of a film of α-Fe_2O_3 grown onto conducting F–SnO_2 glass substrate was recorded. The diffractograms obtained show that the chemical composition of crystalline film corresponds to α-Fe_2O_3 (Hematite) with a pure rhombohedral crystal structure [24] and SnO_2 (Cassiterite). Additional data of diffraction angles, phase and planes of each peak for are also presented in ESI†, Table S1. The UV-vis absorption spectra of (α-Fe_2O_3)-photoanode has also been recorded, revealing that it absorbs radiation at the visible region below 650 nm, see Fig. S3 in ESI†. The translucent brown thin films showed a very strong absorbance, very close to 1 (100% of the light absorbed), in the range 300–525 nm followed by a monotone linear decrease to 0.5 at 650 nm. The absorbance slowly declined to 0.4 at 800 nm (40% of the light absorbed) and did not reach zero, most probably originating from multiple absorption phenomena within the nanocomposite or scattering at the substrate interface. The total reflectance remained at a very low level (5%) within the whole range of wavelength investigated revealing very low amount of light scattering of the film.

Next, we present a complete characterization study of the up-conversion agent used in our photonic approach, that is, solvothermal $NaYF_4$:Yb^{3+},Er^{3+} up-conversion micro-sized particles. The crystalline structure, size and distribution of the $NaYF_4$ particles, as well as the influence of used synthesis methods, were examined through XRD patterns and TEM images. Thus, Fig.3 (bottom images) shows XRD patterns of solvothermal microparticles, where well-defined diffraction peaks corresponding to hexagonal $NaYF_4$ (JCPDS 28-1192) without impurities were observed. It can be clearly seen how diffraction peaks are shifted to higher angles according to different ionic radii (Yb^{3+} 0.985Å, Er^{3+} 1.004Å and Y^{3+} 1.019 Å), supporting the successfully incorporation of dopant ions into crystalline environments. The morphology of of $NaYF_4$-based materials were also analysed by TEM images, see Fig.3 (upper images). Micro-sized cylindrical-shape particles with a relative broad size distribution is observed, and average width and height sizes around 0.45 μm and 1.3 μm, respectively, as it can be extracted from corresponding histogram, see inset in Fig.3.

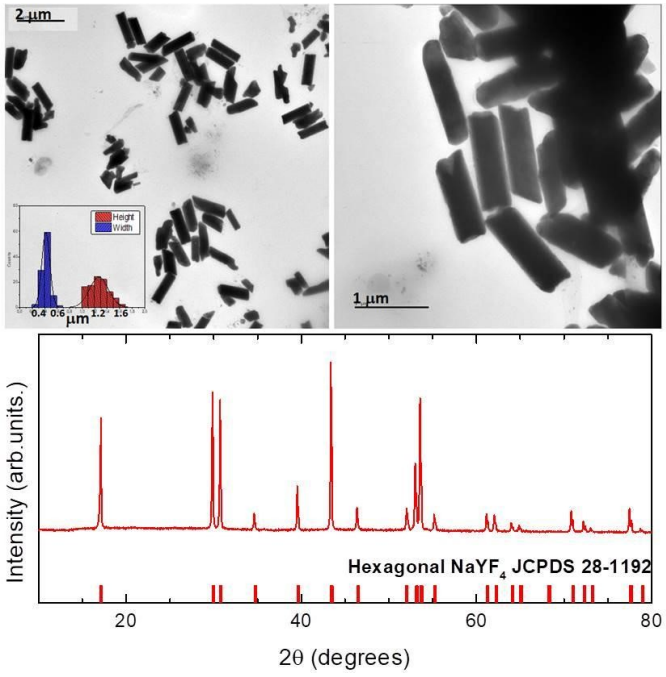

Fig.3 Transmission electron Microscope (TEM) images of $NaYF_4$:5%Yb^{3+}-2%Er^{3+} micro-sized particles Corresponding insets show particle size-distribution histograms (upper images). XRD patterns of solvothermal $NaYF_4$:5%Yb^{3+}-2%Er^{3+} micro-sized particles along with standard data of hexagonal, β-$NaYF_4$, JCPDS 28-1192, (bottom images)

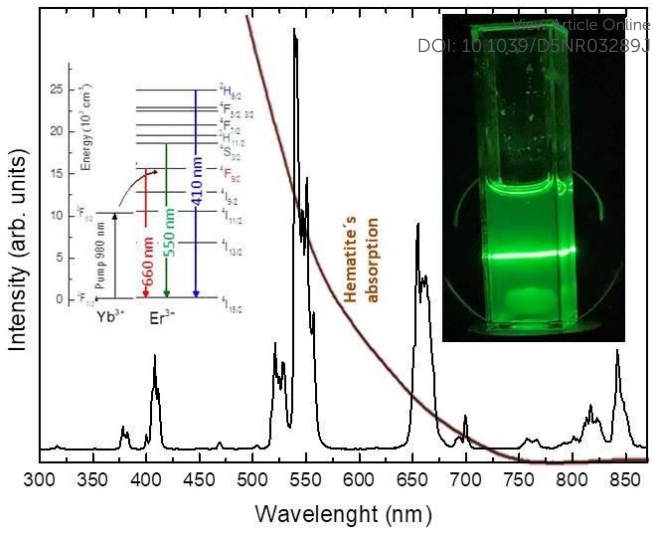

Fig.4 Up-conversion emission spectra of solvothermal $NaYF_4$:5%Yb^{3+}-2%Er^{3+} micro-sized particles under 980 nm laser diode with a power up to 300mW. Inset shows energy level diagrams of Yb^{3+} and Er^{3+} ions with main emission transitions labelled with corresponding wavelengths. A real photograph of up-conversion solvothermal microparticles under infrared excitation is also included. Hematite´s absorbance curve is depicted in red solid line as a reference to show the perfect overlap with green up-conversion emission from rare-earth doped $NaYF_4$ particles.

Up-conversion luminescence

Up-conversion processes are the cornerstones to enable hematite´s photocatalytic activity under infrared excitation by spectral shifting processes. Thus, in Fig. 4 we present up-conversion emission spectra of solvothermal $NaYF_4$:Yb^{3+},Er^{3+} micro-sized particles. The up-converting particles absorb photons in the unused NIR range and emit intense visible radiation which can be absorbed by the hematite to induce photocatalysis. As it can be clearly seen, up-conversion emission bands within 410-660 nm perfectly match the hematite absorption also presented in Fig. S3 in ESI†.

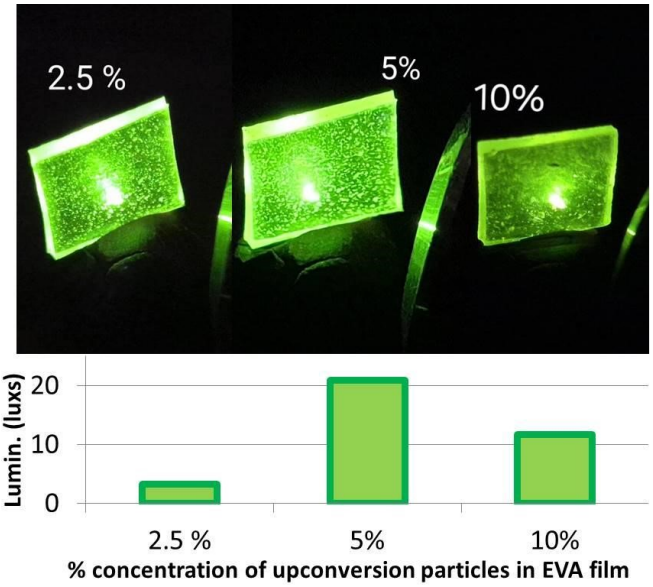

Fig.5 Performance comparison of different concentrations of solvothermal $NaYF_4$:Yb^{3+},Er^{3+} particles embedded in the EVA film, for 2.5, 5 and 10% concentration in weight

According to well-known energy transfer up-conversion mechanisms [3-6], 980 nm NIR photons are efficiently absorbed by Yb^{3+} ions and the absorbed energy is sequentially transferred to Er^{3+} ions, which give rise to red, green and blue emissions located at 660, 550 and 410 nm respectively (see energy level diagrams in the inset of Fig. 4). The large absorption cross-section of Yb^{3+} ions at around 980 nm ($^2F_{7/2}$ → $^2F_{5/2}$ transition) is used as an efficient infrared antenna, resonant with many inexpensive NIR commercial laser diodes.

Therefore, ''up-converted'' photons in the visible range can activate the α-Fe_2O_3 photocatalysts by generating electron-hole pairs to overcome the corresponding bandgap. A real picture of $NaYF_4$:Yb^{3+},Er^{3+}@$NaYF_4$ micro-sized particles emitting quite intense (at naked eye) bright green up-conversion luminescence under 980 nm infrared pump is also presented in Fig. 4.

It is well known that photoluminescence is not a linear process with respect to dopant or particle concentration. Instead, the emission intensity typically increases until reaching an optimal concentration, beyond which it decreases due to different effects. To determine the optimum loading in our system, we systematically prepared and characterized with different microparticle concentrations. This approach allowed us to identify the concentration range that maximizes the up-conversion emission while minimizing detrimental effects. Specifically, the performance of different concentrations of solvothermal $NaYF_4$:Yb^{3+},Er^{3+} particles embedded in the EVA film are presented, for 2.5, 5 and 10% concentration in weight, see Figure 5. An straight-forward luminescence comparison among samples leads us to the selection of EVA films containing 5 wt% NaYF4 particles, as most efficient luminescent sample, and therfore will be used at up-conversion driven photocatalytic water-splitting presented in the following section. At 10% concentration, the microparticles form aggregates within the EVA matrix, which increases optical scattering and creates local shadowing. This reduces the effective excitation volume, as some particles shield others from the incident NIR light. In addition, the reduced interparticle distance can promote cross-relaxation processes between activator ions, leading to further drop in emission efficiency. Similar effects have been reported in the literature for upconversion materials at high concentrations [26-28].

At this point, it should be remarked that there is a full transmittance of the bare EVA polymer within the visible and NIR region of the spectrum (only with high absorption in the UV range below 250 nm), in Fig. S4 in ESI†. Therefore EVA film does not interfere with green and red up-conversion emissions of the $NaYF_4$ particles.

Up-conversion powered hematite's water-splitting

To demonstrate the ability of up-conversion luminescence to indeed achieve infrared-induced water-splitting, next we show evidence of up-conversion driven photocatalytic activity of α-Fe_2O_3 yielding hydrogen generation. For this purpose, we

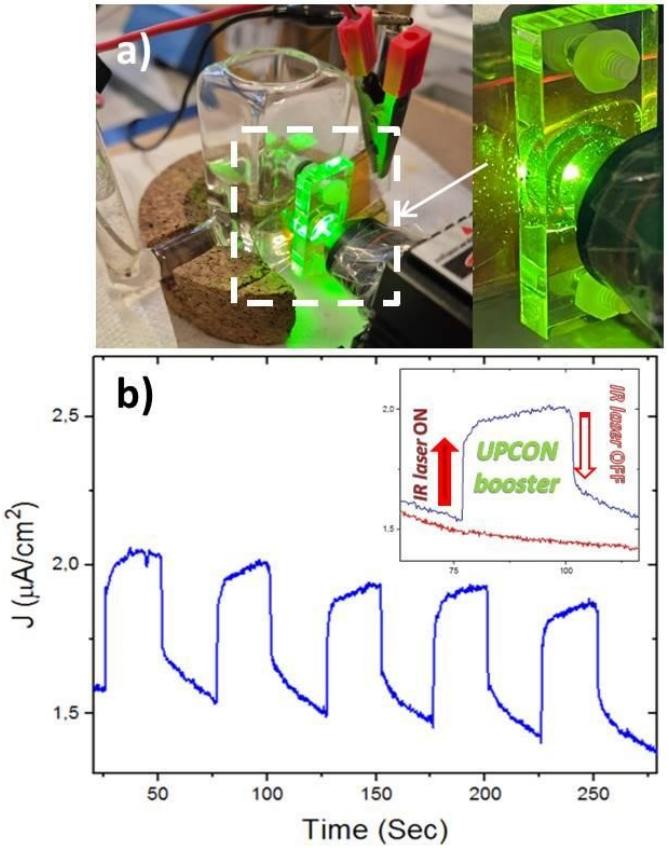

Fig.6 (a) Real picture of the setup of the up-conversion powered PEC cell (b) detailed of luminescent EVA film, containing rare-earth doped $NaYF_4$ particles, laminated over the hematite photoelectrode under 980 nm excitation. (b) Multi-cycle photoanodic current measurements obtained by a low-power NIR laser diode (980 nm) exciting source using solvothermal $NaYF_4$:5%Yb^{3+}-2%Er^{3+} micro-sized particles as up-conversion agent. Inset shows single-cycle experiment along with zero line (red curve) stands for null observed photocurrent in the absence of upconversion particles.

performed photo-electrocatalysis experiments with an original set-up of a Fujishima-Honda cell [5, 7], comprising the synthesized hematite (α-Fe_2O_3)-photoanode aimed at measuring photoanodic currents.

Fig.6 shows the density of current obtained when IR light, from 980 nm laser diode, is focused on luminescent EVA film, containing solvothermal $NaYF_4$:Yb^{3+},Er^{3+}@$NaYF_4$ micro-sized particles, and laminated over the hematite photoelectrode in our PEC set-up for multi-cycle photoanodic current measurements. The detection of a photocurrent generated when 980 nm laser is turned on, as it can be clearly seen in single-cycle in the inset in Figure 6b, labelled as "UPCON booster", confirms the generation of the required electron-hole pairs, and subsequent water-splitting reaction, completely driven by up-converted photons. The incident 980 nm laser light by itself would be unable to activate the semiconductor without these spectral conversion processes. In detail, the mechanism works as follows: The intense green emitted radiation coming out from $NaYF_4$ particles embedded in the EVA film under NIR excitation, generates the oxidation on the α-Fe_2O_3 photocatalyst surface due to the perfect overlap of intense visible up-conversion emission bands (from 410 to 660) and the hematite absorbance, see Fig. 4. This spectral match will overcome photocatalyst bandgap enabling water-splitting and hydrogen generation. Thus, we obtain an "infrared-driven" straightforward activation of the α-Fe_2O_3 photoanode in a Fujishima-Honda PEC cell set-up [5, 7] see Fig. 6a. The photocurrent is measured by the potentiostat taking into account that the exposed surface of the photoelectrode is 0.38 cm^2, as stated in the experimental section. It should be also taking into account that when light is switched on, photogenerated holes accumulate in surface states, and when it's switched off, these trapped charges and intermediates discharge, leading to transient current peaks [29]. Moreover, the photocurrent follows a decay inversely proportional to the square root of time, according to Cottrell's equation [30].

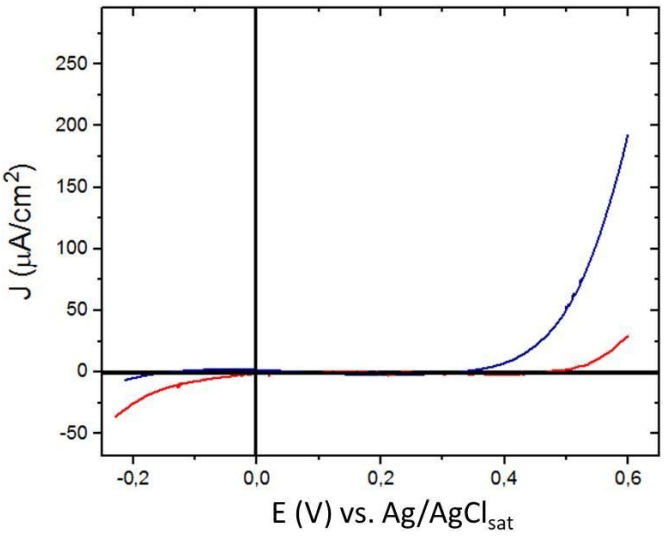

Fig.7 J-V (current-voltage) curves at 5 mV/s, i.e., J ($\mu A/cm^2$) plotted against E (volts) vs. $Ag/AgCl_{sat}$: under 300mW 980 nm laser diode excitation striking rare-earth doped up-converting particles embedded in the EVA film (blue curve) and striking the EVA alone without up-conversion particles (red curve).

Nevertheless, the single-cycle and the multi-cycle experiments presented in Fig, 6b, show a similar reaction profile, corresponding to stationary regime.

Water-splitting reaction is only present while infrared laser is on, and photocurrent goes to zero when the IR source is switched off, giving rise to significant photoanodic currents with the only use of a single low-power IR exciting source (300 mW). This opens the way for indoor applications for photocatalytic processes under low power and low-cost infrared laser diodes, instead of relatively expensive and harmful UV sources [31]. Moreover the photocurrent measurements are not only shown for one single irradiation cycle, but multiple cycles are also included in the inset in Fig.6b. It should be noticed that the obtained values of infrared-driven photocurrent here presented can be even higher, since our set-up configuration could be further optimized with future designs considering the wave-guiding of light into the PEC cell. [4,5]

On the other hand, we have disregard the activation of α-Fe_2O_3 photocatalysts by any other unforeseen effect of the NIR light, or to other thermal effects caused by possible heating due to NIR laser irradiation [5, 18]. In particular, in a control experiment, focusing NIR laser diode over non-luminescent EVA films, where the up-conversion $NaYF_4$ particles were absent, no photocurrent was detected (see zero line in inset in Figure 6b) evidencing that no hydrogen/oxygen evolution was originated.

These control checks should never be underestimated, to avoid misinterpretation of up-conversion sensitized photocatalysis, extensively pointed out in detail by E.L. Cates and co-workers in ref. [18]. In other words, in many recent works, up-conversion effect in photochemistry is largely assumed rather than proven experimentally therein [18]. These control experiments, for example using host material without any up-conversion agent, are crucial to discern between optical or chemical effects.

For that reason, up-conversion driven photocatalysis is here verified as a solely and univocally photonic effect, converting incident NIR radiation before reaching solution reactor [5].

Finally, in order to complete the photoelectrochemical characterization of the presented up-conversion powered PEC cell, the J-V (current-voltage) curves, are also presented in Fig. 7, with and without upconversion particles embedded in the EVA film). It can be clearly observed the effect of the light coming from rare-earth doped up-converting particles embedded in the EVA film (blue curve in Fig. 7) when comparing with the EVA film alone without up-conversion particles (red curve in Fig 7). The photocurrent is noticeably enhanced by the effect of upconversion emission under excitation of 980 nm laser diode, i.e,, blue curve vs red curve in the J-V (current-voltage) presented in Fig. 7.

Thus, harnessing infrared radiation holds promising potentiality for activation of hematite photocatalysts. As the

only light to which α-Fe_2O_3 surface is exposed is the 980 nm laser, we can assure that green up-converted photons are the only responsible, as pure photonic approach to the problem [5]. The incident NIR radiation is converted before it reaches the chemically unmodified α-Fe_2O_3 photocatalysts. This evidences the pure role of the of the photonic up-conversion effect on the NIR-driven boosted hematite's water-splitting.

Conclusions

Here we have proved an up-conversion assisted activation of hematite photocatalysts by rare-earth doped $NaYF_4$ particles embedded into a polymeric EVA film using a simple original Fujishima and Honda PEC cell set-up. And we have made use of one of the most useful, abundant and low cost photoelectrode, that is, the hematite (α-Fe_2O_3). Intense green up-conversion luminescence under 980 nm irradiation has led to generation of a photoanodic current which confirms the photochemical water-splitting reaction on the α-Fe_2O_3 surface, as a solely up-conversion luminescent effect to split water over a hematite´s photoelectrode: *"in rust we shine"*. Moreover the successful integration of up-converting micro-sized rare-earth doped $NaYF_4$ particle into luminescent EVA films, which are used to laminate glass with hematite coated on the opposite side, represents a proof-of-concept and opens the way for indoor applications of this all-in-one photonic device.

Conflicts of interest

There are no conflicts to declare

Data availability

The data supporting this article have been included as part of the Supplementary Information†

Acknowledgements

This work has been financially supported by MAGEC-REEsearch project (ProID2017010078) of "Agencia Canaria de Investigación" (ACIISI) and by Gobierno de Canarias (Proyecto "Tierras raras", Grant number SD- 22/25). It has also been funded by FICYT - Consejería de Ciencia, Innovación y Universidad - Gobierno del Principado de Asturias through the 2018–2022 Science, Technology and Innovation Plan and by the European Union through the European Regional Development Fund (ERDF), Grant number AYUD/2021/57246. Authors want to acknowledge. The authors would like to thank the use of SEGAI-ULL for XRD and TEM measurements.

Notes and references

1 D.G. Nocera, *Acc. Chem. Res*., 2012, **45**, 767 (1-10).
2 J. P. Torella et al., *Proc. Natl. Acad. Sci*., 2015, **112**, 2337.
3 L. Wondraczek, E. Tyystjärvi, J. Méndez-Ramos, F. A. Müller and Q. Zhang, *Adv. Sci*., 2015, **2**, 1500218.
4 J. Méndez-Ramos, P. Acosta-Mora, J. C. Ruiz-Morales, T. Hernández, M. E. Borges and P. Esparza, *RSC Adv.,* 2013, **3**, 23028.
5 J. Méndez-Ramos, M.E. Borges, S. Torres-García, M. Medina-Alayón, P. Acosta-Mora, J. del-Castillo, A. Menéndez-Velázquez, C.B. Mullins, P. Esparza, *Journal of Power Sources*, 2025, **625**, 235668.
6 J. de Wild, A. Meijerink, J. K. Rath, W. G. J. H. M. van Sark and R. E. I. Schropp, *Energy Environ. Sci*., 2011, **4**, 4835.
7 A. Fujishima and K. Honda, *Nature*, 1972, **238**, 37.
8 P. Acosta-Mora, K. Domen, T. Hisatomi, H. Lyu, J. Méndez-Ramos, J. C. Ruiz-Morales and N. M. Khaidukov, *Chem. Commun*. 2018, **54**, 1905.
9 D.K. Bora, A.Braun and E.C. Constable, *Energy Environ. Sci*., 2013, **6**, 407.
10 Y. Lin, G. Yuan, S. Sheehan, S. Zhou, y D. Wang, *Energy Environ. Sci.*, **2011**, 4, 12, 4862.
11 H. Liu, X. Fan, Y. Li, H. Guo, W. Jiang, y G. Liu, *J. Environ. Chem. Eng*., 2023, **11**, 1, 109224.
12 K. Sivula, F. Le Formal, y M. Grätzel, *Chem. Sust. Chem*, 2011, 4, **4**, 432.
13 F. Gonell, M. Haro, R. S. Sánchez, P. Negro, I. Mora-Seró, J. Bisquert, B. Julián-López, S. Giménez, *J. Phys. Chem. C*, 2014, **118**, 21, 11279.
14 C. Pornrungroj, Virgil Andrei and E. Reisner, *J. Am. Chem. Soc.* 2023, 145, **25**, 13709.
15 J. Méndez-Ramos, J. C. Ruiz-Morales, P. Acosta-Mora, J. del-Castillo and A.C. Yanes, *Journal of Power Sources*, 2013, **238**, 313.
16 M. Zhang, Y. Lin, T.J. Mullen, W.-F. Lin, L.-D. Sun, C.-H. Yan, T. E. Patten, D. Wang, G.-Y. Liu, J. Phys. Chem. Lett., 2012, 3, 21, 3188.
17 M.E. Borges, H. de Paz Carmona, M. Gutiérrez, P. Esparza *Catalysts* 2023, **13**(6), 1023.
18 S.P. Sahu, S.l. Cates, H.-I. Kim, J.-H.J. Kim, E.L. Cates, *Environ. Sci. Technol.,* 2018, **52**, 2973.
19 J. Wang, R. Li, Z. Zhang, W. Sun, R. Xu, Y.Xie, Z. Xing, X. Zhang, *Applied Catalysis A*, 2008, **334**, 227.
20 J. Wang, Y. Xie, Z. Zhang, J. Li, X. Chen, L. Zhang, R. Xu, X. Zhang, *Solar Energy Materials & Solar Cells*, 2009, **93**, 355.
21 J. del-Castillo, J. Méndez-Ramos, P. Acosta-Mora and A.C. Yanes, *Journal of Luminescence*, 2022, **241**, 118490.
22 K. Aitola, G. Gava Sonai, M. Markkanen, J. Kaschuk, X. Hou, K. Miettunen, K, P.D. Lund, *Solar Energy* 2022, **237**, 264.
23 A.B. García-Delgado, A. Menéndez-Velázquez, J. Méndez-Ramos, S. Torres-García, M. Medina-Alayón, P. Acosta-Mora, J. del-Castillo, M.E. Borges, P. Esparza, *Journal of Luminescence* 2024, **273**, 120671.
24 L. Vayssieres, J. Guo, J. Nordgren, *Journal of Nanoscience and Nanotechnology* 2001, **1**, 385.
25 J. Mathew, N. Nirmala, *International Journal on Applied Bioengineering* 2015, **9**, 36.
26 Jones, C.M.S.; Panov, N.; Skripka, A.; Gibbons, J.; Hesse, F.; Bos, J.-W.G.; Wang, X.; Vetrone, F.; Chen, G.; Hemmer, E.; et al. *Opt. Express*, 2020, **28**, 22803
27 Chen, B.; Wang, F, *Acc. Chem. Res*. 2020, **53**, 358.
28 Wang, Z.; Meijerink, A., *J. Phys. Chem. C* 2018, **122**, 26298.
29 Liu, S. and Xu, Y.-J., *Scientific Reports*, 2016, **6**, 22742.
30 J.C. Myland, K.B. Oldham*, Electrochemistry Communications* 2004, **6**, (4), 344.
31 A. Santana-Alonso, A.C. Yanes, J. Méndez-Ramos, J. del-Castillo and V.D. Rodríguez, *Optical Materials* 2011, **33**, 587.

View Article Online
DOI: 10.1039/D5NR03289J

Data availability

The data supporting this article have been included as part of the Supplementary Information†